

# Group theory analysis of electrons and phonons in N-layer graphene systems

L. M. Malard, D. L. Mafra, M. H. D. Guimarães, M. S. C. Mazzoni and A. Jorio  
*Departamento de Física, Universidade Federal de Minas Gerais, 30123-970, Belo Horizonte, Brazil*

(Dated: December 6, 2008)

In this work we study the symmetry properties of electrons and phonons in graphene systems as function of the number of layers. We derive the selection rules for the electron-radiation and for the electron-phonon interactions at all points in the Brillouin zone. By considering these selection rules, we address the double resonance Raman scattering process. The monolayer and bilayer graphene in the presence of an applied electric field are also discussed.

PACS numbers: 02.20.-a, 78.30.-j, 78.67.-n

## I. INTRODUCTION

The current interest on graphene and its multilayered materials has been stimulated by various experimental and theoretical works addressing the physics of Dirac fermions and the potential for device applications ([1, 2] and references therein). Group theory is a powerful theoretical tool to determine eigenvectors, the number and the degeneracies of eigenvalues and to obtain and understand the selection rules governing, for example, electron-radiation and electron-phonon interactions. Although the symmetry aspects of mono-layer graphene and graphite have been largely discussed in the literature [3], the recent findings generate interest in a group theory analysis depending on the number of graphene layers.

This work presents a group theory analysis for electrons and phonons in mono-, bi- and tri-layer graphene, extending for N layers depending if N is even or odd. The selection rules for electron-radiation interaction within the dipole approximation and for electron scattering by phonons are derived. With these selection rules, we discuss the double-resonance Raman (DRR) scattering process, which has been widely used to characterize the number of layers [4, 5, 6] and to probe their electronic and vibrational properties [7, 8, 9]. Finally, we also discuss the differences when mono- and bi-layer graphene are exposed to external electrical fields, giving insight on the gap opening in the biased bilayer graphene [10, 11, 12, 13] and different selection rules for the electron-phonon scattering (EPS) process.

Section II gives the symmetry properties for mono-layer and N layer graphene depending if N is even or odd. The monolayer and bilayer graphene are also considered in the presence of an electric field perpendicular to the graphene plane. The notation adopted is related to the space group symmetry, and conversion to the point group notation can be found in the appendix. Section III presents the selection rules for the electron-radiation interaction. Section IV shows the  $\Gamma$  point Raman and infrared active modes, and we extend the electron-phonon selection rules to points in the interior of the Brillouin zone in section V. Considering both sections III and V we address the DRR process for mono-, bi- and tri-layer graphene in section VI. The main findings are summa-

rized in section VII.

## II. SYMMETRY PROPERTIES

### A. Group of wavevector

Figure 1(a,d) shows the hexagonal real space for the monolayer graphene with two inequivalent atoms in the unit cell. The origin is set at the highest symmetry point, i.e. at the center of a hexagon. The reciprocal space is shown in Fig. 1(g) highlighting the high symmetry points  $\Gamma$ , K, K', M and lines T, T',  $\Sigma$ . Any other generic point outside the high symmetry lines and points is named here  $u$ . The monolayer graphene on an isotropic medium has the space group  $P6/mmm$  ( $D_{6h}^1$ ) in the Hermann-Mauguin notation. At the  $\Gamma$  point, the group of wavevector (GWV) is isomorphic to the point group  $D_{6h}$  (the Schoenflies character tables for the point groups can be found in Ref. [3]).

The real space for bilayer and trilayer graphene with AB Bernal stacking are shown in Figs. 1(b,e) and (c,f), respectively. The symmetries for N-layer graphene, with N even or odd (from now on,  $N \neq 1$ ), are the same of bilayer and trilayer graphene, respectively. The main symmetry operation distinguishing the point groups between even and odd layers are the horizontal mirror plane, which is absent for N even, and the inversion, which is absent for N odd. The point groups isomorphic to the GWV for mono-, N-layer graphene (N even and odd), and for N infinite (graphite) are listed in table I for all points and lines in the first Brillouin Zone (BZ). The GWV for N-layers graphene are subgroups of the GWV for single layer graphene. The direct product between the group from N even and N odd gives the graphene GWV, i.e.

$$\{G_{even}|0\} \otimes \{G_{odd}|0\} = \{G_{monolayer}|0\}.$$

On graphite, the wavevector point groups are isomorphic to the wavevector point groups of monolayer graphene, but differ fundamentally for some classes where a translation of  $c/2$  is present, graphite belonging to the  $P6_3/mmc$  ( $D_{6h}^4$ ) non-symorphic space group.

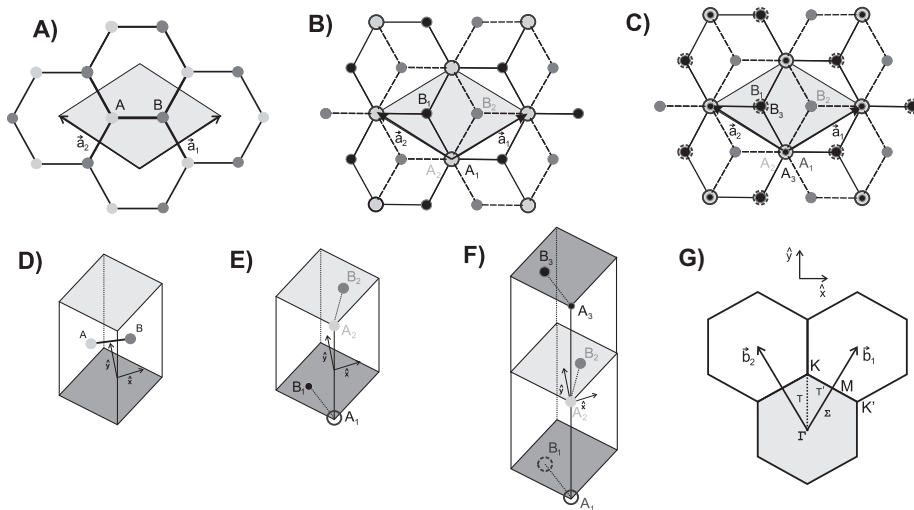


FIG. 1: (a) The real space top-view of a monolayer graphene showing the non-equivalent A and B atoms. (b) The real space top-view of bilayer graphene. Light and dark gray dots, and black circles and dots represent the atoms in the upper and lower layers, respectively. (c) The real top-view trilayer graphene. Small and large black dots, light and dark gray dots, and traced and solid circles represent the atoms in the upper, middle and lower layers, respectively. The unit cell of the (d) monolayer, (e) bilayer and (f) trilayer graphene. (g) The reciprocal space showing the 1<sup>st</sup> Brillouin zone in light gray, the high symmetry points and lines and the two primitive vectors.

TABLE I: The space groups and wavevector point groups for mono-, N-layer graphene and graphite at all points in the BZ.

	Space group	$\Gamma$	K (K')	M	T (T')	$\Sigma$	u
Monolayer	P6/mmm	D <sub>6h</sub>	D <sub>3h</sub>	D <sub>2h</sub>	C <sub>2v</sub>	C <sub>2v</sub>	C <sub>1h</sub>
N even	P3m1	D <sub>3d</sub>	D <sub>3</sub>	C <sub>2h</sub>	C <sub>2</sub>	C <sub>1v</sub>	C <sub>1</sub>
N odd	P6m2	D <sub>3h</sub>	C <sub>3h</sub>	C <sub>2v</sub>	C <sub>1h</sub>	C <sub>2v</sub>	C <sub>1h</sub>
N infinite	P6 <sub>3</sub> /mmc	D <sub>6h</sub>	D <sub>3h</sub>	D <sub>2h</sub>	C <sub>2v</sub>	C <sub>2v</sub>	C <sub>1h</sub>

## B. Lattice vibrations and $\pi$ electrons

The representations for the lattice vibration ( $\Gamma_{lat.vib.}$ ) and for the  $\pi$  electrons ( $\Gamma_{\pi}$ ) are given by  $\Gamma_{lat.vib.} = \Gamma^{eq} \otimes \Gamma^{vector}$  and  $\Gamma_{\pi} = \Gamma^{eq} \otimes \Gamma^z$ , respectively, where  $\Gamma^{eq}$  is the atom equivalence representation,  $\Gamma^{vector}$  is the representation for the vectors  $x$ ,  $y$  and  $z$ . For  $\Gamma_{\pi}$  we used only  $\Gamma^z$ , which is the irreducible representation for the vector  $z$ , since  $\pi$  electrons in graphene are formed by  $p_z$  electronic orbitals. The results for all points and lines in the first BZ for the  $\Gamma_{lat.vib.}$  are found in Table II and for the  $\Gamma_{\pi}$  in Table III.

Table III shows that the  $\pi$  electrons in monolayer graphene are degenerated at the K (Dirac) point, as obtained by theory [14]. Figures 2(a), (b) and (c) show the electronic structure of a mono-, bi- and tri-layer graphene, respectively calculated via density functional theory (DFT) [15, 16, 17]. The symmetry assignments of the different electronic branches shown in Fig. 2 were made according to the DFT projected density of states.

The bilayer graphene with AB Bernal stacking [see Fig. 1(b,e)] is also a zero gap semiconductor composed by two conduction and two valence bands, and the electrons exhibit a parabolic dispersion near the K point.

Two bands are degenerated at the K point (see Table III and Fig. 2(b)) and the other two have a gap of  $2\gamma_1$ , where  $\gamma_1$  is the Slonczewski-Weiss-McClure parameter [18, 19] that have a experimental value of  $\sim 0.3 - 0.4\text{eV}$  [7, 10, 20].

Trilayer graphene in the ABA Bernal stacking (see Fig. 1(c,f)), belongs to the D<sub>3h</sub> point group and Fig. 2(c) shows its electronic dispersion. The K point of trilayer is isomorphic to C<sub>3h</sub>. In Tables II and III,  $K_2^+$  and  $K_2^{+*}$  are the two one-dimensional representations of the  $K_2^+$  representation, where  $*$  means the complex conjugate. The same happens for the  $K_2^-$  representation. The electron representations will be given by  $\Gamma_{\pi}^K = K_1^+ + 2K_1^- + K_2^{+*} + K_2^- + K_2^{-*}$  for the K point and  $\Gamma_{\pi}^{K'} = K_1^+ + 2K_1^- + K_2^+ + K_2^{-*} + K_2^-$  for K' point. Although time reversion symmetry can imply degeneracy between complex conjugate representations in cyclic groups, in graphene the complex conjugation also takes K into K' point and, consequently, there are no degenerated bands at the K (K') point, in agreement with *tight-binding* calculations when including the  $\gamma_2$  and  $\gamma_5$  next-nearest-layer coupling parameters [21, 22]. This energy gap is also obtained from *ab initio* calculations (see the inset of Fig. 2 (c) and Ref. [23]).

## C. Gated mono- and bi-layer graphene

If the monolayer graphene is in the presence of a perpendicular electric field (gated graphene), the Fermi level changes. The presence of charge inhomogeneity caused by substrate and/or absorbed water can generate the same effect as verified in transport [24, 25] and Raman measurements [26], where the Dirac point is shifted from

TABLE II: The  $\Gamma_{lat.vib.}$  wavevector point-group representations for mono- and N-layer graphene at all points in the BZ.

	Monolayer	N even	N odd
$\Gamma$	$\Gamma_2^- + \Gamma_5^- + \Gamma_4^+ + \Gamma_6^+$	$N(\Gamma_1^+ + \Gamma_3^+ + \Gamma_2^- + \Gamma_3^-)$	$(N-1)\Gamma_1^+ + (N+1)\Gamma_2^- + (N+1)\Gamma_3^+ + (N-1)\Gamma_3^-$
$\mathbf{K}$	$K_1^+ + K_2^+ + K_3^+ + K_3^-$	$N(K_1 + K_2 + 2K_3)$	$NK_1^+ + NK_1^- + [f(N) + 2]K_2^+ + [f(N-2)]K_2^{+*} + NK_2^- + (N-1)K_2^{-*}$ <sup>a</sup>
$\mathbf{M}$	$M_1^+ + M_2^+ + M_3^+ + M_2^- + M_3^- + M_4^-$	$N(2M_1^+ + M_2^+ + M_1^- + 2M_2^-)$	$2NM_1 + (N-1)M_2 + (N+1)M_3 + 2NM_4$
$\mathbf{T}(\mathbf{T}')$	$2T_1 + T_2 + 2T_3 + T_4$	$3N(T_1 + T_2)$	$(3N+1)10T^+ + (3N-1)T^-$
$\Sigma$	$2\Sigma_1 + 2\Sigma_3 + 2\Sigma_4$	$N(4\Sigma_1 + 2\Sigma_2)$	$2N\Sigma_1 + (N-1)\Sigma_2 + (N+1)\Sigma_3 + 2N\Sigma_4$
$\mathbf{u}$	$4u^+ + 2u^-$	$6Nu$	$(3N+1)u^+ + (3N-1)u^-$

<sup>a</sup>Where  $f(N) = \sum_{m=0}^{\infty} [\Theta(N-4m-2) + 3\Theta(N-4m-4)]$ , where  $\Theta(x)$  is equal to 0 if  $x < 0$  and equal 1 otherwise.

TABLE III: The  $\Gamma_\pi$  wavevector point-group representations for mono- and N-layer graphene at all points in the BZ.

	Monolayer	N even	N odd
$\Gamma$	$\Gamma_2^- + \Gamma_4^+$	$N(\Gamma_1^+ + \Gamma_2^-)$	$(N-1)\Gamma_1^+ + (N+1)\Gamma_2^-$
$\mathbf{K}(\mathbf{K}')$	$K_3^-$	$\frac{N}{2}(K_1 + K_2 + K_3)$	$(\frac{N-1}{2})K_1^+ + (\frac{N+1}{2})K_1^- + g(N)K_2^{+*}(K_2^+) + g(N-2)(K_2^+)(K_2^{+*}) + g(N)K_2^- + g(N+2)K_2^{-*}$ <sup>a</sup>
$\mathbf{M}$	$M_3^+ + M_2^-$	$N(M_1^+ + M_2^-)$	$(N-1)M_1 + (N+1)M_4$
$\mathbf{T}(\mathbf{T}')$	$T_2 + T_4$	$N(T_1 + T_2)$	$(N-1)T^+ + (N+1)T^-$
$\Sigma$	$2\Sigma_4$	$2N\Sigma_1$	$(N-1)\Sigma_1 + (N+1)\Sigma_4$
$\mathbf{u}$	$2u^-$	$2Nu$	$(N-1)u^+ + (N+1)u^-$

<sup>a</sup>Where  $g(N) = \sum_{m=0}^{\infty} \Theta(N-4m-2)$ , where  $\Theta(x)$  is equal to 0 if  $x < 0$  and equal 1 otherwise.

the neutrality point. In this case, the  $\pi$  electrons lose the horizontal mirror plane and the inversion symmetry, and the system is isomorphic to the point group  $C_{6v}$ . The irreducible representations for the  $\Gamma_\pi$  for the gated graphene can be found in Table IV. There is no gap opening at K point for a perfect perpendicular electric field effect.

The biased bilayer graphene have attracted a lot of attention recently because it is the only material known to have a tunable energy gap [10, 11, 12, 13], promising for applications on devices and lasers with tunable energy. The mechanism behind this feature is based on applying an electric field perpendicular to the graphene layers, so that the two layers will be under an inequivalent potential. Then it is possible to open a gap at the K point, breaking the double degenerated  $K_3$  irreducible representation into two one-dimensional irreducible representations. Since the biased bilayer graphene breaks the inversion center symmetry, the group of the wavevector at  $\Gamma$  for perfect perpendicular electric field is isomorphic to  $C_{3v}$ . Table IV shows that the biased bilayer contains the two one-dimensional representations  $K_2$  and  $K_2^*$  at the K point, then a gap opening is expected on the basis of symmetry arguments of inequivalent layers.

The representations for the  $\Gamma_{lat.vib.}$  of the gated monolayer (or biased bilayer) are the same as the monolayer (or bilayer) in an isotropic medium, given in table II. The electric field does not affect the symmetries of the phonons.

### III. SELECTION RULES FOR ELECTRON-RADIATION INTERACTION

The symmetry properties described in the previous section will now be applied to physical processes. In this sec-

TABLE IV: The group of wavevector and its  $\Gamma_\pi$  representations for gated monolayer and biased bilayer graphene.

	Gated monolayer		Biased Bilayer	
	GWV	$\Gamma_\pi$	GWV	$\Gamma_\pi$
$\Gamma$	$C_{6v}$	$\Gamma_1 + \Gamma_4$	$C_{3v}$	$4\Gamma_1$
$\mathbf{K}(\mathbf{K}')$	$C_{3v}$	$K_3$	$C_3$	$2K_1 + K_2 + K_2^*$
$\mathbf{M}$	$C_{2v}$	$M_1 + M_3$	$C_{1v}$	$4M_1$
$\mathbf{T}(\mathbf{T}')$	$C_{1v}$	$T_1 + T_2$	$C_1$	$4T$
$\Sigma$	$C_{1v}$	$2\Sigma_1$	$C_{1v}$	$4\Sigma_1$
$\mathbf{u}$	$C_1$	$2u$	$C_1$	$4u$

tion we discuss the selection rules for electron-radiation interaction in the dipole approximation, with emphasis on the high symmetry lines T and T' in the electronic dispersion, where interesting phenomena occur.

In the dipole approximation, the absorption of light in a material is related to the wave functions of the electron states in the valence ( $\psi^v(\mathbf{k})$ ) and conduction ( $\psi^c(\mathbf{k})$ ) bands and the polarization of the incoming light ( $\mathbf{P}$ ) by  $W(\mathbf{k}) \propto |\mathbf{P} \cdot \langle \psi^c(\mathbf{k}) | \nabla | \psi^v(\mathbf{k}) \rangle|^2$  [27, 28]. Knowing the symmetry of the initial and final states, and the representation that generates the basis function of the light polarization vector ( $x$ ,  $y$  or  $z$ ), group theory can be used to compute whether  $W(\mathbf{k})$  is null or not. The results are summarized in Table V considering graphene layers lying in the  $(x,y)$  plane and light propagating along  $z$ . In the case of graphene, the light absorption up to 3 eV occurs only at T, T' and  $u$  points.

It is important to highlight some results given in Table V. In the case of monolayer graphene on an isotropic medium, numerical calculations show an anisotropy in the optical absorption [28, 29, 30]. This anisotropy has indeed a symmetry basis, as clearly seen when analyzing the selection rules at the T line. Absorption by visible light has to couple  $T_2$  and  $T_4$   $\pi$  electron symmetries (see Fig. 2(a)). For the T line direction along  $\hat{y}$ , the only

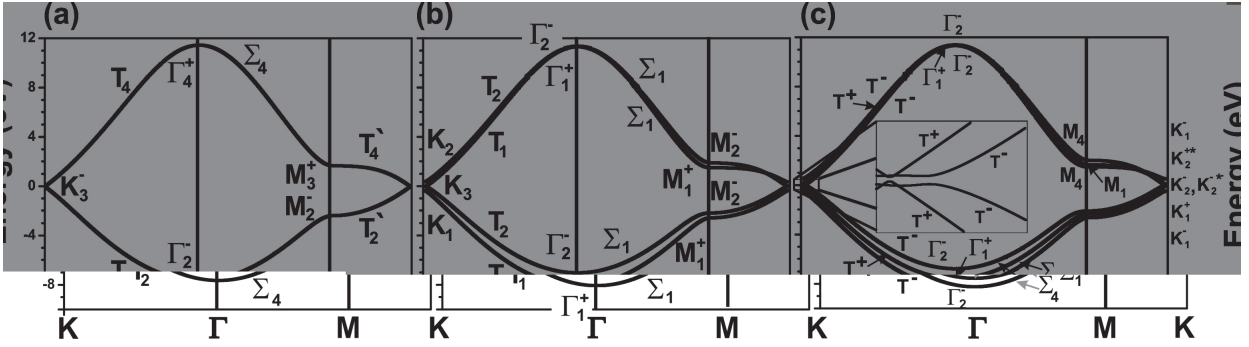


FIG. 2: The electronic dispersion for the  $\pi$  electrons calculated by DFT and the irreducible representations ( $\Gamma_\pi$ ) for (a) monolayer, (b) bilayer and (c) trilayer along the K $\Gamma$ MK directions. The calculation was done via pseudopotential DFT [15] as implemented in the SIESTA program [16, 17]. We used a basis set composed of pseudo atomic orbitals of finite range and the Local Density Approximation (LDA) with the Ceperley-Alder parametrization for the exchange-correlation functional.

TABLE V: Selection rules for electron-radiation interaction with  $\hat{x}$  and  $\hat{y}$  light polarization in mono-, bi- and tri-layer (see Fig. 1 (g) for  $\hat{x}$  and  $\hat{y}$  definition). For N even and N odd the selection rules are the same as for bi- and tri-layer graphene, respectively.

	BZ point	polarization	$W(\mathbf{k})$
monolayer	T	$x \in T_3$ $y \in T_1$	$T_2 \otimes T_3 \otimes T_4$ non null $T_2 \otimes T_1 \otimes T_4$ null
	$u$	$x, y \in u^+$	$u^- \otimes u^+ \otimes u^-$ non null
gated monolayer	T	$x \in T_2$ $y \in T_1$	$T_1 \otimes T_2 \otimes T_2$ non null $T_1 \otimes T_1 \otimes T_2$ null
	$u$	$x, y \in u$	$u \otimes u \otimes u$ non null
bilayer (N-even)	T	$x \in T_2$	$T_1 \otimes T_2 \otimes T_1$ null
			$T_1 \otimes T_2 \otimes T_2$ non null
	$y \in T_1$	$T_2 \otimes T_2 \otimes T_2$ null	
		$T_1 \otimes T_1 \otimes T_1$ non null $T_1 \otimes T_1 \otimes T_2$ null $T_2 \otimes T_1 \otimes T_2$ non null	
$u$	$x, y \in u$	$u \otimes u \otimes u$ non null	
biased bilayer	T	$x, y \in T$	$T \otimes T \otimes T$ non null
	$u$	$x, y \in u$	$u \otimes u \otimes u$ non null
trilayer (N-odd)	T	$x, y \in T^+$	$T^+ \otimes T^+ \otimes T^+$ non null
			$T^+ \otimes T^+ \otimes T^-$ null
	$u$	$x, y \in u^+$	$u^+ \otimes u^+ \otimes u^+$ non null $u^+ \otimes u^+ \otimes u^-$ null $u^- \otimes u^+ \otimes u^-$ non null

allowed absorption is for light polarized along the  $\hat{x}$  direction. For incident light polarization along the  $\hat{y}$  direction, no absorption will occur along K $\Gamma$  direction, giving rise to the optical absorption anisotropy on graphene [28, 29, 30]. Outside the high symmetry T line there is a non-zero probability of absorption and the anisotropy is obtained by defining orthogonal basis, as shown in Ref. [28].

When the monolayer graphene is on top of a substrate, with the influence of the environment changing the Fermi level, there will be no change in the selection rules for electron-radiation interaction. Along the T line, the  $\pi$  electrons are described by  $T_1$  and  $T_2$  representations,

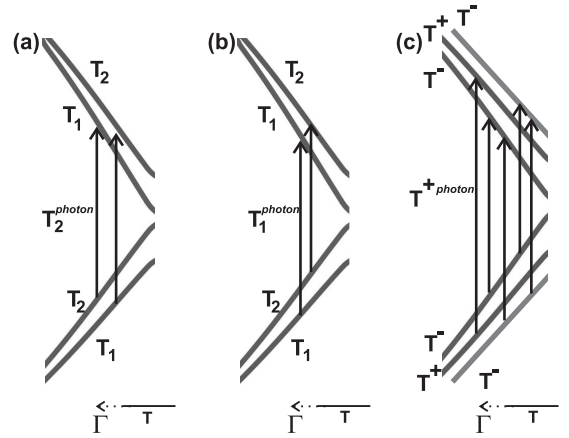


FIG. 3: (a,b) Schematic electron dispersion of bi-layer graphene along the K $\Gamma$  direction showing the possible transition induced by (a) a photon with  $T_2$  symmetry ( $x$  polarization) and (b) a  $T_1$  photon ( $y$  polarization). (c) The electronic dispersion of tri-layer graphene showing the five possible transitions by light absorption.

where  $T_2$  and  $T_1$  contain  $x$  and  $y$  basis function, respectively. Again there will be no absorption for  $y$  polarization.

The bilayer graphene is composed by four electronic bands at the T line, belonging to two  $T_1$  and two  $T_2$  irreducible representations. The four possible transitions are illustrated in Fig. 3 (a,b). In this case both  $x$  and  $y$  polarized light can be absorbed. For the biased bilayer graphene, all electronic representations are the same, and it contains both  $x, y$  base functions for light polarizations. Thus, all the four transitions are allowed connecting all the four bands by the same light polarization, differently from the unbiased bilayer case where the light polarization selects the pair of bands that can be connected.

The trilayer graphene will have more possibilities for light induced transitions, since there are more possibil-

ities between the three  $\pi$  and three  $\pi^*$  bands. Along  $T(T')$  direction, there are two  $T^+$  and four  $T^-$  bands giving rise to five possible transitions (see Table V), as shown in Fig. 3 (c).

#### IV. SELECTION RULES FOR THE FIRST-ORDER RAMAN SCATTERING AND INFRARED ABSORPTION PROCESSES

The first-order Raman scattering process is limited to phonons at the center of BZ ( $\Gamma$  point) due to momentum conservation requirement (phonon wavevector  $q = 0$ ). In monolayer graphene the first-order Raman spectra is composed by the G band vibrational mode, which is doubly degenerated at the  $\Gamma$  point with  $\Gamma_6^+$  symmetry. The Raman active modes depending on N ( $N > 1$ ) (without acoustic modes) are:

$$\Gamma^{\text{Raman}} = N(\Gamma_3^+ + \Gamma_1^+), \text{ for N even}$$

$$\Gamma^{\text{Raman}} = N\Gamma_3^+ + (N - 1)(\Gamma_3^- + \Gamma_1^+), \text{ for N odd}$$

For even number of layers the G band belongs to the  $\Gamma_3^+$ . There is a low frequency  $\Gamma_3^+$  mode with frequency depending on the number of layers ( $35\text{-}53 \text{ cm}^{-1}$ )[31]. Two new Raman active modes near  $\sim 80 \text{ cm}^{-1}$  and  $\sim 900 \text{ cm}^{-1}$  appear with  $\Gamma_1^+$  irreducible representations [31, 32]. For odd number of layers the G band is assigned as a combination of  $\Gamma_3^+$  and  $\Gamma_3^-$  representations, also the smaller wavenumber component is active in Raman by a  $\Gamma_1^+$  representation.

For monolayer graphene there is an infrared (IR) active mode belonging to the  $\Gamma_2^-$  representation, giving rise to an absorption near  $\sim 870 \text{ cm}^{-1}$ . The IR active modes for  $N > 1$  are:

$$\Gamma^{\text{IR}} = (N - 1)\Gamma_2^- + (N - 1)\Gamma_3^-, \text{ for N even}$$

$$\Gamma^{\text{IR}} = N(\Gamma_3^+ + (\Gamma_2^-)), \text{ for N odd}$$

For even number of layers the active modes belong to the  $\Gamma_2^-$  and  $\Gamma_3^-$  representations, the later one referring to the  $\sim 1590 \text{ cm}^{-1}$  frequency vibration [31, 32]. The infrared active modes for odd layer number belong to  $\Gamma_2^-$  and  $\Gamma_3^+$  which are also Raman active.

#### V. ELECTRON SCATTERING BY $q \neq 0$ PHONONS

The electron-phonon scattering (EPS) is calculated from the initial and final electron wave functions coupled by the phonon eigenvector [33, 34] using the phonon-induced deformation potential. Therefore, the selection rules of the EPS processes are obtained by the direct product of the symmetries of the initial and final electronic states and the symmetry of the phonon involved

in the process. The allowed electron-phonon scattering processes for monolayer, gated monolayer, bilayer, biased bilayer and trilayer graphene along the  $K\Gamma$  and  $KM$  directions ( $T$  and  $T'$ , lines respectively) and at a generic  $u$  point are summarized in Table VI.

TABLE VI: Allowed processes for electron-phonon scattering for mono-, bi- and tri-layer graphene along the  $T$  and  $T'$  lines and at a generic  $u$  point for each phonon symmetry. For N even and N odd the selection rules are the same as for bi- and tri-layer graphene, respectively.

	BZ point	phonon	allowed scattering
monolayer	$T(T')$	$T_1$	$T_2 \rightarrow T_2, T_4 \rightarrow T_4$
		$T_3$	$T_2 \rightarrow T_4$
	$u$	$u^+$	$u^- \rightarrow u^-$
gated monolayer	$T(T')$	$T_1$	$T_1 \rightarrow T_1, T_2 \rightarrow T_2$
		$T_2$	$T_1 \rightarrow T_2$
	$u$	$u$	$u \rightarrow u$
bilayer (N-even)	$T(T')$	$T_1$	$T_1 \rightarrow T_1, T_2 \rightarrow T_2$
		$T_2$	$T_1 \rightarrow T_2$
	$u$	$u$	$u \rightarrow u$
biased bilayer	$T(T')$	$T$	$T \rightarrow T$
		$u$	$u \rightarrow u$
	$u$	$u$	$u \rightarrow u$
trilayer (N-odd)	$T(T')$	$T^+$	$T^+ \rightarrow T^+, T^- \rightarrow T^-$
		$T^-$	$T^+ \rightarrow T^-$
	$u$	$u^+$	$u^+ \rightarrow u^+, u^- \rightarrow u^-$
		$u^-$	$u^+ \rightarrow u^-$

#### VI. DOUBLE RESONANCE RAMAN SCATTERING PROCESS

One example of explicit use of the electron-radiation and EPS selection rules is the double resonance Raman scattering process [35, 36], in which an electron in the conduction band is scattered by a phonon with wavevector outside the  $\Gamma$  point in an intervalley (connecting electronic states near the K and  $K'$  points) or in an intravalley (connecting electronic state near the same K or  $K'$  point) process. The  $G'$  Raman band ( $\sim 2700 \text{ cm}^{-1}$ ) comes from an intervalley process in which the electron is scattered by an in-plane transversal optic (iTO) phonon. We will discuss in details the  $G'$  scattering for mono- and multi-layer graphene.

For the monolayer graphene, the possible scattering is illustrate in Fig. 4. The iTO phonon at the  $KM$  ( $T'$ ) direction presents a  $T_1$  symmetry [37], which can only connect two electrons with the same symmetry. Many other similar scattering events are allowed by symmetry, involving electron in the  $K\Gamma$  ( $T$ ) direction or at any general  $u$  point inside the circle defined by the  $T_3$  photon energy. However, the matrix element has a strong angular dependence and the scattering is dominated by the T electrons, as discussed in Ref. [9]. Therefore, the  $G'$  Raman band has only one peak, with full width at half maximum (FWHM) of  $\sim 24 \text{ cm}^{-1}$  (see Fig. 6 (a)) [4, 9]. For the graphene on top of a substrate, the same selection rules apply, and the expected number of  $G'$  peaks is the same as for the isolated monolayer graphene on an

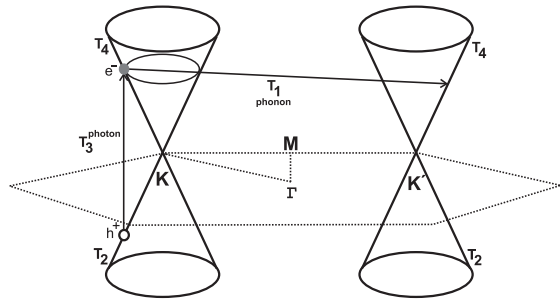


FIG. 4: The most efficient DRR process in graphene showing the absorption of light with polarization symmetry  $T_3$  followed by electron scattering by a phonon with  $T_1$  symmetry.

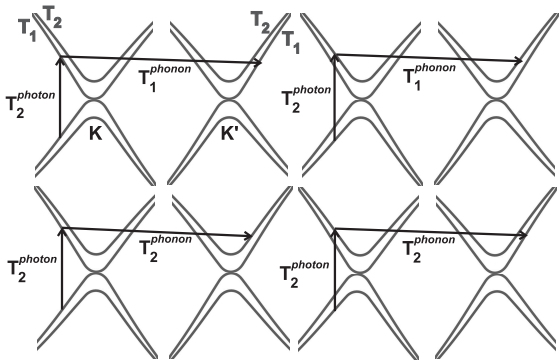


FIG. 5: The four allowed DRR processes in bilayer graphene, taking into account the optical anisotropy.

isotropic medium.

For the bilayer graphene, the number of allowed DRR processes predicted by group theory will be larger, since both electronic and phonon branches are doubled. Along the T line, there is polarization dependence for the absorption linking different electronic bands, as discussed in section III. For wavevectors in the range of visible light energy, the electron dispersion are almost linear, then optical anisotropy can be applied here as for monolayer graphene [38]. Now, for computing the number of resonant conditions involved in the DRR process, we are left with only two excited electronic bands with symmetries  $T_1$  and  $T_2$ , which corresponds to Fig. 3 (a). The  $i$ TO phonons for bilayer graphene have  $T_1$  and  $T_2$  symmetries. For the electron scattering by a  $T_1$  phonon, the allowed processes are between K and  $K'$  electronic bands with same symmetry ( $T_1 \rightarrow T_1$  or  $T_2 \rightarrow T_2$ ). The same happens with the electron scattering by a  $T_2$  phonon, but it connects conduction bands of different symmetries, i.e.  $T_1 \rightleftharpoons T_2$ . This gives rise to four possible DRR processes, as shown in Fig 5 [4]. The Raman spectra can then be used to differentiate mono- and bi-layer graphene (see Fig. 6)[4, 5, 6].

In the case of biased bilayer graphene, there are no selection rules involving different photon polarizations.

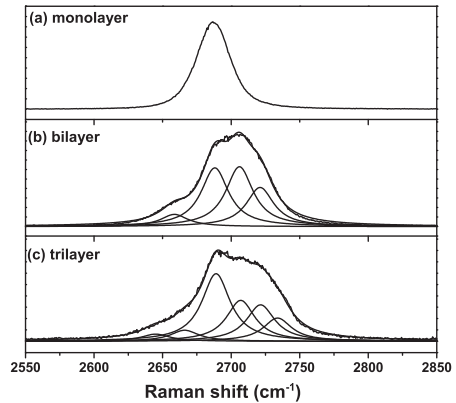


FIG. 6: The measured Raman spectra of the  $G'$  band of a (a) mono- (b) bi- and (c) trilayer graphene. The samples were made by exfoliating graphite on top of a 100 nm silicon oxide substrate using 2.41 eV laser energy. The  $G'$  band for mono- bi- and tri-layer graphene were fitted with 1, 4 and 6 Lorentzians, respectively, with a FWHM of  $24 \text{ cm}^{-1}$ .

The biased bilayer can have photon absorption linking all valence and conduction bands. This leads to eight possible transitions considering EPS selection rules for  $T_1$  and  $T_2$  phonons.

For the trilayer graphene, the DRR process will have again more contributions because each phonon and electron band will be split in three levels. Along the T line, there are five possibilities linking the electronic bands between the K and  $K'$  points with a  $T^+$  phonon, and four possibilities for the  $T^-$  phonon. The total number of DRR process predicted by group theory will be fifteen. However, the FWHM is large when compared to the energy splitting between the  $G'$  Raman peaks, and when one makes measurements of the  $G'$  Raman band, these fifteen peaks cannot be distinguished, as illustrated in Fig. 6. Similar problem should happen for  $N \geq 4$ .

## VII. SUMMARY

In this work we analyzed the symmetry aspects related to electrons and phonons at each point in the BZ of graphene, depending on the number of layers. The symmetry aspects can be generalized to any value of  $N$ , differing for  $N$  even or odd. For monolayer and bilayer we consider both an isotropic and an anisotropic medium. We derived the selection rules for electron-radiation and electron-phonon interactions. Some specific findings can be remarked:

- For the monolayer graphene, the predicted optical anisotropy [28] comes out directly from group theory analysis. The electron-phonon scattering process is allowed by symmetry at any generic point ( $u$ ) in the Dirac cone, and the observation of a single Lorentzian in the  $G'$  Raman band comes from a strong anisotropy in the electron-phonon matrix element [9].

- The gated graphene have lower symmetry, but the optical anisotropy is still present, and for the DRR process, the symmetry considerations are the same as graphene on an isotropic medium.

- In the case of bilayer graphene, the optical anisotropy is also present and there are four dominant processes in the DRR. This number increases to eight on biased bilayer.

- In trilayer graphene, the number of possible DRR processes is fifteen. However, the 15 processes are not distinguishable and the  $G'$  Raman band can be nicely fit with 6 Lorentzians. Similar situation is expected for larger number of layers.

### Acknowledgements

L.M.M, D.L.M and M.H.D.G contributed equally for this work and acknowledge the Brazilian agency CNPq. This work was supported by Rede Nacional de Pesquisa em Nanotubos de Carbono - MCT, FAPEMIG, CNPq and Capes. We would like to thank M. A. Pimenta, L. G. Cançado, E. B. Barros and R. W. Nunes for useful

discussions.

### APPENDIX: NOTATION CONVERSION FROM SPACE GROUP TO POINT GROUP IRREDUCIBLE REPRESENTATIONS

In this work we derived the  $\Gamma_\pi$  and  $\Gamma_{lat.vib}$  for all points in the first BZ of multilayer graphene maintaining the notation of space group (SG) for the irreducible representations. The conversion to point group (PG) representation is obtained considering that (**a**) superscript sign “+” or “-” applies if the character of the horizontal mirror ( $\sigma_h$ ) or inversion ( $i$ ) is positive or negative, respectively; (**b**) the subscript number is given following the order of the point group irreducible representations; (**c**) two representations can only have the same number if they have superscript with positive or negative signs. As an example we give in Table VII the  $\Gamma$  point space group notation conversion to the  $D_{3h}$  (N-odd) and  $D_{3d}$  (N-even) point groups and for the K point space group to the  $C_{3h}$  (N-odd) and  $D_3$  (N-even) point groups.

- 
- [1] A. K. Geim and K. S. Novoselov, Nature Materials **6**, 183 (2007).
  - [2] A. H. Castro Neto, F. Guinea, N. M. R. Peres, K. S. Novoselov and A. K. Geim, arXiv:0709.1163 (2007).
  - [3] M. S. Dresselhaus, G. Dresselhaus and A. Jorio, *Group Theory: Application to the Physics of Condensed Matter* (Springer-Verlag, Heidelberg, 2008).
  - [4] A. C. Ferrari, J. C. Meyer, V. Scardaci, C. Casiraghi, M. Lazzeri, F. Mauri, S. Piscanec, D. Jiang, K. S. Novoselov, S. Roth, and A. K. Geim, Phys. Rev. Lett. **97**, 187401 (2006).
  - [5] A. Gupta, G. Chen, P. Joshi, S. Tadigadapa, P. C. Ekland, Nano Lett. **6**, 2667 (2006).
  - [6] D. Graf, F. Molitor, K. Ensslin, C. Stampfer, A. Jungen, C. Hierold and L. Wirtz, Nano Lett. **7**, 238 (2007).
  - [7] L. M. Malard, J. Nilsson, D. C. Elias, J. C. Brant, F. Plentz, E. S. Alves, A. H. Castro Neto, and M. A. Pimenta, Phys. Rev. B **76**, 201401 (2007).
  - [8] Z. Ni, Y. Wang, T. Yu, Y. You and Z. Shen, Phys. Rev. B **77**, 235403 (2008).
  - [9] D. L. Mafra, G. Samsonidze, L. M. Malard, D. C. Elias, J. C. Brant, F. Plentz, E. S. Alves, and M. A. Pimenta, Phys. Rev. B **76**, 233407 (2007).
  - [10] T. Ohta, A. Bostwick, T. Seyller, K. Horn and E. Rotenberg, Science **313**, 951 (2006).
  - [11] E. V. Castro, K. S. Novoselov, S. V. Morozov, N. M. Peres, J. M. dos Santos, J. Nilsson, F. Guinea, A. K. Geim, and A. H. Neto, Phys. Rev. Lett. **99**, 216802 (2007).
  - [12] E. McCann, Phys. Rev. B **74**, 161403(R) (2006).
  - [13] J. Nilsson, A. H. Castro Neto, F. Guinea, N. M. R. Peres, Phys. Rev. B **76**, 165416 (2007).
  - [14] R. Saito, G. Dresselhaus, and M. S. Dresselhaus, *Physical Properties of Carbon Nanotubes* (Imperial College

TABLE VII: Example of irreducible representation notation conversion from the  $\Gamma$  point space group to  $D_{3h}$  and  $D_{3d}$  point groups, and from the K point space group to  $C_{3h}$  and  $D_3$  point groups.

$\Gamma$ point				K point			
$D_{3h}$		$D_{3d}$		$C_{3h}$		$D_3$	
SG	PG	SG	PG	SG	PG	SG	PG
$\Gamma_1^+$	$A_1'$	$\Gamma_1^+$	$A_{1g}$	$K_1^+$	$A'$	$K_1$	$A_1$
$\Gamma_1^-$	$A_1''$	$\Gamma_1^-$	$A_{1u}$	$K_1^-$	$A''$	$K_2$	$A_2$
$\Gamma_2^+$	$A_2'$	$\Gamma_2^+$	$A_{2g}$	$K_2^+$	$E'$	$K_3$	$E$
$\Gamma_2^-$	$A_2''$	$\Gamma_2^-$	$A_{2u}$	$K_2^{+*}$	$E'^*$		
$\Gamma_3^+$	$E'$	$\Gamma_3^+$	$E_g$	$K_3^+$	$E''$		
$\Gamma_3^-$	$E''$	$\Gamma_3^-$	$E_u$	$K_3^{+*}$	$E''^*$		

- [15] W. Kohn and L.J. Sham, Phys. Rev. **140** A1133 (1965).
- [16] P. Ordejón, E. Artacho and J.M. Soler, Phys. Rev. B **53**, R10441 (1996).
- [17] J. M. Soler, E. Artacho, J. D. Gale, A. Garcia, J. Junquera, P. Ordejón and D. Sánchez-Portal, J. Phys.: Condens. Matter **14** 2745 (2002).
- [18] J. W. McClure, Phys. Rev. **108**, 612 (1957).
- [19] J. C. Slonczewski and P. R. Weiss, Phys. Rev. **109**, 272 (1958).
- [20] T. Ohta, A. Bostwick, J. L. McChesney, T. Seyller, K. Horn, and E. Rotenberg, Phys. Rev. Lett. **98**, 206802 (2007).
- [21] M. Koshino and E. McCann, arXiv:0809.0983 (2008).
- [22] B. Partoens and F. M. Peeters, Phys. Rev. B **74**, 075404 (2006).
- [23] S. Latil and L. Henrard, Phys. Rev. Lett. **97**, 036803 (2006).

- [24] K. S. Novoselov, A. K. Geim, S. V. Morozov, D. Jiang, Y. Zhang, S. V. Dubonos, I. V. Grigorieva and A. A. Firsov, *Science* **306**, 666 (2004).
- [25] Y. Zhang, Y. Tan, H. L. Stormer and P. Kim, *Nature* **438**, 201 (2005).
- [26] C. Casiraghi, S. Pisana, K. S. Novoselov, A. K. Geim, and A. C. Ferrari, *Appl. Phys. Lett.* **91**, 233108 (2007).
- [27] P. Y. Yu and M. Cardona, *Fundamentals of Semiconductors: Physics and Materials Properties* (Springer-Verlag, Heidelberg, 2005).
- [28] A. Grüneis, R. Saito, Ge. G. Samsonidze, T. Kimura, M. A. Pimenta, A. Jorio, A. G. Souza Filho, G. Dresselhaus, and M. S. Dresselhaus, *Phys. Rev. B* **67**, 165402 (2003).
- [29] L. G. Cançado, M. A. Pimenta, B. R. Neves, G. Medeiros-Ribeiro, T. Enoki, Y. Kobayashi, K. Takai, K. Fukui, M. S. Dresselhaus, R. Saito, and A. Jorio, *Phys. Rev. Lett.* **93**, 047403 (2004).
- [30] L. G. Cançado, M. A. Pimenta, B. R. Neves, M. S. Dantas, and A. Jorio, *Phys. Rev. Lett.* **93**, 247401 (2004).
- [31] S. K. Saha, U. V. Waghmare, H. R. Krishnamurthy and A. K. Sood, *Phys. Rev. B* **78**, 165421 (2008).
- [32] J. Jiang, H. Tang, B. Wang and Z. Su, *Phys. Rev. B* **77**, 235421 (2008).
- [33] J. Jiang, R. Saito, A. Grüneis, S. G. Chou, Ge. G. Samsonidze, A. Jorio, G. Dresselhaus, M. S. Dresselhaus, *Phys. Rev. B* **71**, 205420 (2005).
- [34] A. H. Castro Neto and F. Guinea, *Phys. Rev. B* **75**, 045404 (2007).
- [35] C. Thomsen and S. Reich, *Phys. Rev. Lett.* **85**, 5214 (2000).
- [36] R. Saito, A. Jorio, A. G. Souza Filho, G. Dresselhaus, M. S. Dresselhaus and M. A. Pimenta, *Phys. Rev. Lett.* **88**, 027401 (2002).
- [37] J. Maultzsch, S. Reich, C. Thomsen, H. Requardt and P. Ordejón, *Phys. Rev. Lett.* **92**, 075501 (2004).
- [38] L. G. Cançado, A. Reina, J. Kong and M. S. Dresselhaus, *Phys. Rev. B* **77**, 245408 (2008).